New Insights into ^{99}Tc(VII) Removal by Pyrite: A Spectroscopic Approach

Diana M. Rodríguez, Natalia Mayordomo,* Andreas C. Scheinost, Dieter Schild, Vinzenz Brendler, Katharina Müller,* and Thorsten Stumpf

ABSTRACT: ^{99}Tc(VII) uptake by synthetic pure pyrite at 21 °C was studied in a wide pH range from 3.50 to 10.50 using batch experiments combined with scanning electron microscopy, X ray absorption spectroscopy (XAS), X ray photoelectron spectroscopy (XPS), and Raman microscopy. We found that pyrite removes Tc quantitatively from solution ($\log K_d$ = 5.0 ± 0.1) within 1 day at pH ≥ 5.50 ± 0.08. At pH < 5.50 ± 0.08, the uptake process is slower, leading to 98% Tc removal ($\log K_d$ = 4.5 ± 0.1) after 35 days. The slower Tc uptake was explained by higher pyrite solubility under acidic conditions. After 2 months in contact with oxygen at pH 6.00 ± 0.07 and 10.00 ± 0.04, Tc was neither reoxidized nor redissolved. XAS showed that the uptake mechanism involves the reduction from Tc(VII) to Tc(IV) and subsequent inner sphere complexation of Tc(IV)−Tc(IV) dimers onto a Fe oxide like hematite at pH 6.00 ± 0.07, and Tc(IV) incorporation into magnetite via Fe(III) substitution at pH 10.00 ± 0.04. Calculations of Fe speciation under the experimental conditions predict the formation of hematite at pH < 7.50 and magnetite at pH > 7.50, explaining the formation of the two different Tc species depending on the pH. XPS spectra showed the formation of TcS_x at pH 10.00 ± 0.04, being a small fraction of a surface complex, potentially a transient phase in the total redox process.

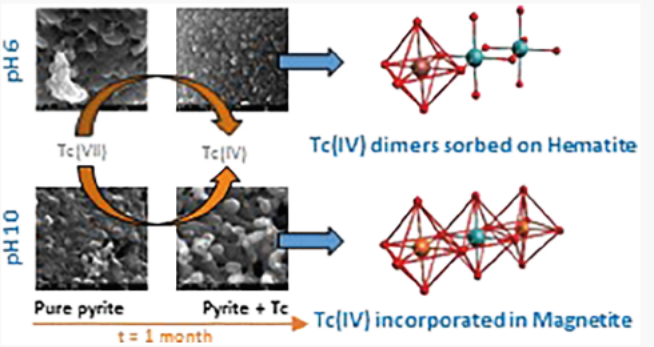

INTRODUCTION

Technetium (Tc), the lightest element with no stable isotopes, is found on earth mainly due to anthropogenic sources.[1] It is produced in nuclear power plants as a fission product of ^{235}U and ^{239}Pu,[2,3] while other techniques, such as Tc generators from ^{99}Mo, are used to provide ^{99m}Tc for medical applications.[4,5] Furthermore, nuclear weapon testing has caused major environmental Tc contamination during the last century.[1,3] Although most of Tc isotopes have short half lives (less than 100 days), ^{99}Tc is a weak β particle emitter with a long half life (2.14×10^5 years) that can be incorporated into living organisms through the consumption of contaminated water or food. In humans, ^{99}Tc is mainly localized in the thyroid gland (75%), gastrointestinal tract (20%), and liver (5%), and the biological half lives for Tc in these locations are 1.6, 3.7, and 22 days, respectively.[6] When the dose exceeds 0.04 mSv per year, it can cause cancer and other health problems.[7] Therefore, it is crucial to establish strategies for Tc immobilization before it can reach the biosphere and efficient remediation measures once ^{99}Tc has entered it.

Technetium migration behavior and bioavailability depend strongly on its speciation in aqueous solution, which is highly influenced by the redox conditions.[1,2,8] Under oxidizing conditions, Tc mainly exists as Tc(VII) in the form of pertechnetate, TcO_4^-, a highly water soluble anion that hardly sorbs on minerals or sediments[9] and its groundwater migration is favored in consequence. Under reducing conditions, Tc(VII) becomes Tc(IV), whose main species, TcO_2, is a poorly water soluble solid with significantly lower mobility than pertechnetate. Other oxidation states of Tc require stabilization by ligands that are hardly encountered in natural environments.[1]

Several studies approach Tc(VII) reductive immobilization using minerals containing reducing Fe(II), such as magnetite ($Fe^{II}Fe_2^{III}O_4$)[10] or mackinawite (FeS),[10−13] that are commonly found in the environment. The authors have confirmed the Tc(VII) reduction triggered by Fe^{2+} (and S^{2-}) and subsequent Tc(IV) retention on the mineral surfaces. However, as the reoxidation of Tc(IV) is thermodynamically favored in contact with O_2, i.e., under atmospheric conditions, mere precipitation of TcO_2 is not sufficient for water remediation.[14−19] Therefore, an effective mineral for Tc removal would promote its

structural incorporation by processes like structural diffusion or coprecipitation, or form strong inner sphere sorption complexes with it, to avoid Tc remobilization.

Pyrite is widely distributed throughout the earth in geological formations such as sedimentary deposits, hydrothermal veins, and metamorphic rocks, and it is the most common redox sensitive sulfur mineral with a large pH stability range from 2 to 10.[20] As iron sulfides are accessory minerals in crystalline and clay rocks, which are considered as potential host rocks for nuclear waste repositories,[21,22] pyrite has been identified as a good scavenger for ^{99}Tc(VII) from soil and groundwater in both the presence[23] and absence[24,25] of humic substances. However, the pH effect on the Tc immobilization is not clear since the studies were reported in a relatively narrow pH range from 4 to 7. In addition, although it can be inferred from studies with other Fe(II) minerals that Tc retention on pyrite should be due to the reduction from Tc(VII) to Tc(IV), it is not known whether Tc(IV) is incorporated, precipitated, or sorbed on the mineral surface. The specific molecular mechanisms triggered by pyrite need to be determined to allow the design and optimization of a sustainable and efficient retardation strategy for Tc contamination.

We have studied the reductive immobilization of ^{99}Tc(VII) by synthetic pure pyrite with the aim of understanding the effect of pH, Tc loading, and ionic strength on the process and identifying the mechanisms responsible for the Tc removal. Tc batch contact experiments were carried out over wide parameter ranges (pH from 3.50 to 10.50, contact time from 1 to 42 days, initial Tc concentrations from 2×10^{-7} to 2×10^{-3} M in water, and 0.1 M NaCl) under oxygen exclusion at 21 °C. Additionally, anoxic batch experiments at pH 6.00 and 10.00 were subsequently exposed to oxygen to evaluate the reoxidation of Tc(IV). Scanning electron microscopy helped to analyze the morphology of the pyrite before and after Tc interaction. X ray absorption spectroscopy, X ray photoelectron spectroscopy, and Raman microscopy were used to identify the Tc retention mechanisms and the molecular environments after its interaction with pyrite.

MATERIALS AND METHODS

Radiation Safety. ^{99}Tc is a β particle emitter with a long half life (2.14×10^5 years) and should be handled only in a dedicated radiochemistry laboratory with specific radiation safety measurements in place. The possession and use of radioactive materials is regulated by statutory laws.

Pyrite. Synthetic iron sulfide, FeS_2 (Alfa Aesar), was used. The mineral characterization experiments were carried out under a N_2 atmosphere in a glovebox (GS050912, GS Glovebox System; <1 ppm O_2). The grain size of the pyrite was 50 μm (found by scanning electron microscopy, SEM) and its Brunauer−Emmet−Teller specific surface area was determined to be 2.0 $m^2\ g^{-1}$ by isotherm experiments with N_2 at 77 K (Multipoint Beckman Coulter surface analyzer SA 3100). The X ray diffractogram (MiniFlex 600 powder XRD, Rigaku) confirmed its purity (RRUFF database[26] reference R050190). Raman spectra (Aramis, Horiba) of the powder also coincided very well with this pure pyrite R050190 reference. Both XRD and Raman microscopy rule out marcasite (orthorhombic FeS_2) contamination (Figure S1a,b). The isoelectric point (pH_{IEP}) was determined at pH 7.90 by carrying out ζ potential measurements (Zetasizer Nano Series Nano ZS, Malvern Instruments) of suspensions under varying pH values (Figure S1c). This pH_{IEP} value indicates that the pyrite surface was initially oxidized, i.e., presenting Fe(III) moieties.[27] However, we refrained from an initial acid washing treatment of the used pyrite sample, because environmental pyrite surfaces show Fe(III) moieties as well.[28]

Batch Experiments. All preparations were conducted in a N_2 glovebox (GS050912, GS Glovebox System; <1 ppm O_2) and all aqueous solutions were prepared under a N_2 atmosphere with Milli Q water (resistivity = 18.2 MΩ cm, Water Purified) boiled for 2 h, sealed to avoid the oxygen entry, and cooled down at room temperature before its introduction into the glovebox. In general, a suspension of 1.3 ± 0.2 g L^{-1} of pyrite was prepared in water or 0.1 M NaCl ($NaCl_{(s)}$ from Merck, purity ≥ 99%) depending on the experiment. The required amount of 9.22×10^{-3} M $K^{99}TcO_4$ stock solution (by courtesy of the Institute of Radiopharmacy at HZDR) was added, and the pH was adjusted with solutions ranging from 2 to 0.02 M HCl or NaOH. The pH of the samples was adjusted regularly two times a week as it changed around ±0.15 pH units every 3−4 days, possibly due to pyrite oxidation.[27] More details on the pH adjustment are given in the Supporting Information. The system was agitated for hours or days on a horizontal shaker. After the distinct contact time, pH and Eh were measured without further stirring of the suspension (equilibrium time for Eh measurement: 30 min).

Table 1 summarizes the set conditions for the batch experiments performed.

Table 1. Conditions of the Batch Experiments

experiment	kinetics	pH effect	isotherm
$[Tc(VII)]_0$ (M)	5.0×10^{-6}	5.0×10^{-6}	2×10^{-7} to 2×10^{-3}
pH	3.50 10.50	3.50 10.50	6.00 and 10.00
contact time (days)	1 42	1 42	14

The supernatant was separated by ultracentrifugation ($2.4 \times 10^5 g$ for 1 h). Then, 250 μL aliquots of the supernatant were mixed with 5 mL of scintillation cocktail (Ultima Gold, Perkin Elmer) to determine the Tc concentration in a solution by liquid scintillation counting (1414 LSC Winspectral α/β Wallac, Perkin Elmer; detection limit: 25 cpm. Measuring time: 10 min). The Tc retained by pyrite as a percentage of Tc and as the K_D value was calculated by applying eqs 1 and 2.

$$\%Tc_{removed} = \frac{([Tc]_0 - [Tc]_t)}{[Tc]_0} \times 100 \quad (1)$$

$$K_D = \frac{([Tc]_0 - [Tc]_t)}{[Tc]_t} \times \frac{V}{m} \quad (2)$$

where $[Tc]_0$ is the initial Tc concentration in the system (in Bq mL^{-1}), $[Tc]_t$ is the concentration of Tc remaining in solution (in Bq mL^{-1}) after certain time (t) of contact, V is the volume of suspension (in mL), and m is the mass of pyrite (in g).

Reoxidation. Two suspensions of pyrite in water (1.3 g L^{-1}) were prepared inside the glovebox at pH 6.00 and 10.00, both containing 5.0×10^{-6} M $K^{99}TcO_4$. The final volume of the samples was 35 mL, and they were stored in 50 mL polypropylene tubes. They were kept under constant agitation for 5 days. At this point, Tc concentration in solution was measured as described in the previous section. It verified the complete retention of Tc at both pH values. Consecutively,

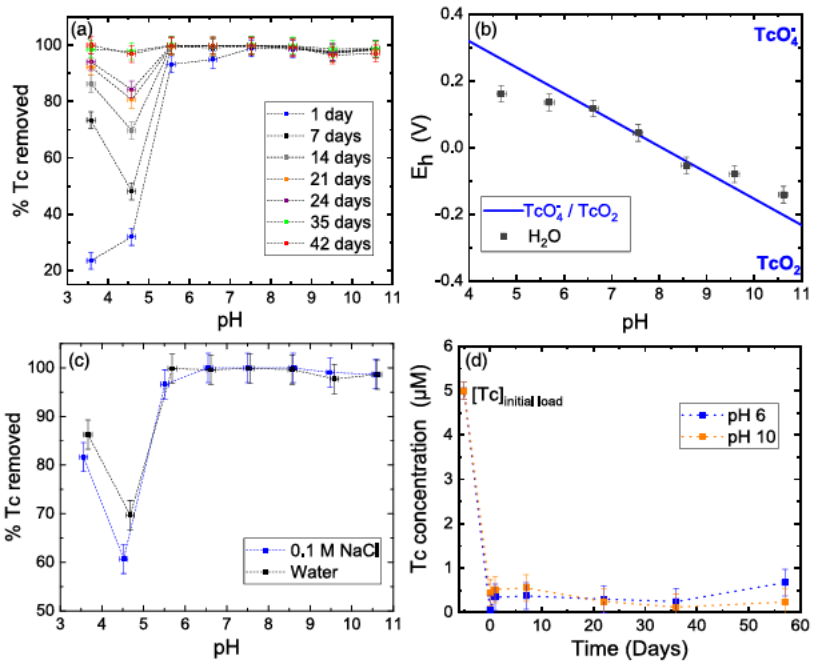

Figure 1. Batch experiments of ^{99}Tc(VII) removal by pure synthetic pyrite. (a) pH effect on the ^{99}Tc(VII) uptake by pyrite for 42 days. (b) Eh − pH diagram of the system Tc + pyrite in water after 14 days of contact and calculated equilibrium line between TcO_4^- and TcO_2. (c) Effect of 0.1 M NaCl on the ^{99}Tc(VII) uptake by pyrite after 14 days in contact. (d) Tc(IV) reoxidation experiments at pH 6.00 ± 0.07 and 10.00 ± 0.04 for 2 months. Dashed lines are shown to guide the eye.

the tubes were opened outside the glovebox under an environmental atmosphere and constant stirring for 1 h; they were closed again and were left on a horizontal shaker for 60 days outside the glovebox. As in the batch experiments, the pH of the samples was adjusted two times a week. Suspensions were regularly sampled by taking 5 mL aliquots to quantify the Tc concentration in the supernatant by LSC, as described before.

Scanning Electron Microscopy (SEM). The sample preparation was performed inside the glovebox. A total of 0.140 g of pyrite was mixed with 50 mL of water, and $K^{99}TcO_4$ was added to obtain ≈1000 and 600 ppm of Tc load in the final solid (Tc initial concentration = 0.048 and 0.028 mM, respectively). The pH was adjusted to 6.00 and 10.00, and the samples were left for equilibration for a month on a horizontal shaker (the pH was also adjusted two times a week during this month). Afterward, the solid was separated by ultracentrifugation ($2.4 \times 10^5 g$ for 1 h) and distributed for separate SEM, X ray photoelectron spectroscopy (XPS), X ray absorption spectroscopy (XAS), and Raman microscopy measurements.

Two blanks of pyrite suspensions in water (1.3 g L^{-1}) were prepared at pH 6.00 and 10.00, left on the horizontal shaker for 1 month, and the pH was adjusted occasionally. They were measured at the same conditions as the ^{99}Tc containing samples.

An FEI Quanta 650 FEG environmental scanning electron microscope was applied to image the sample surfaces. SEM−energy dispersive X ray (SEM EDX) spectra of selected areas were acquired using a Thermo Scientific UltraDry, i.e., Peltier cooled, silicon drift X ray detector and the NORAN System7 microanalysis system, software version 3.3. The sample preparation, as well as the SEM EDX experiments, were carried out under anoxic conditions.

X-ray Absorption Spectroscopy (XAS). The samples used for these experiments come from the preparation described in the SEM section. After ultracentrifugation, the wet pastes for XAS (X ray absorption near edge structure, XANES, and extended X ray absorption fine structure, EXAFS) were mounted on doubly sealed plastic sample holders inside the glovebox. To ensure inert conditions, they were taken outside the glovebox and immediately flash frozen with liquid nitrogen and then stored in a liquid nitrogen container for transportation. Spectra were acquired at the KARA Synchrotron Radiation Source at KIT in fluorescence mode at the Tc K edge (21 044 eV) in a step of 0.5 eV for XANES and with a 0.05 $Å^{-1}$ step for EXAFS up to 12.5 $Å^{-1}$. The measurements were performed at 15 K in a He filled cryostat. The energy of the Si(111) double crystal monochromator was calibrated using a Mo foil (K edge at 20 000 eV). Two Rh coated mirrors were used to collimate the beam into the monochromator crystal and to reject higher order harmonics. Fluorescence spectra were collected with a 13 element, high purity, solid state Ge detector (Canberra) with a digital spectrometer (XIA XMAP). Normalization, transformation from energy into k space, subtraction of a spline background, and shell fits were performed with WinXAS following standard procedures.[29] All fits were carried out in R space (1−3.5 Å) of k^3 weighted spectra (2.0−11.5 $Å^{-1}$ providing a shell resolution of 0.17 Å) using theoretical backscattering amplitudes and phase shifts calculated with FEFF 8.2[30] on clusters (R_{max} = 8 Å) derived from magnetite[31] and TcO_2[32] structures, Tc was placed into the central 6 coordinated Fe position of the former to produce Tc doped magnetite, and replacing part of backscattering Tc atoms by Fe for the latter structure to produce a model for Tc−Tc dimer sorption complexes. The Debye−Waller factor was restricted to float between 0.002 and 0.012 $Å^{-1}$. Furthermore, spectra were analyzed by the iterative transformation factor analysis (ITFA) software package developed by Roßberg.[33] The procedure is well described in several

papers.[10,34] Shortly, the derivation of the number of spectral components is based on three factors, the minimum of the Malinowski indicator value calculated for all principal components, a visual inspection of the principal components to discriminate the ones that contain the EXAFS signal from those that arise from fluctuations of the spline background removal and noise, and finally, and perhaps most important, the reconstruction of the experimental data by a minimum number of components. Varimax rotation and iterative transformation target test modules are then used to identify the spectral endmembers and to extract their EXAFS spectra.

X-ray Photoelectron Spectroscopy (XPS). The samples used for these experiments come from the preparation described in the SEM section. The wet paste was redissolved in ≈1 mL of water. The vials with the samples were always transported and measured under an inert gas atmosphere (N_2 and Ar).

Samples were prepared on indium foil by applying a drop of suspension. The dried samples were mounted onto a sample holder and moved into the XPS device using a transfer vessel and without air contact.

XPS measurements were performed by an XPS system (PHI 5000 VersaProbe II, ULVAC PHI Inc.) equipped with a scanning microprobe X ray source (monochromatic Al Kα (1486.7 eV) X rays). Survey scans of the conductive samples were recorded with an X ray source power of 32 W and pass energy of the analyzer of 187.85 eV. Narrow scans of the elemental lines were recorded at 23.5 eV pass energy, which yields an energy resolution of 0.67 eV FWHM at the Ag $3d_{5/2}$ elemental line of pure silver. Calibration of the binding energy scale of the spectrometer was performed using well established binding energies of elemental lines of pure metals (monochromatic Al Kα: Cu $2p_{3/2}$ at 932.62 eV, Au $4f_{7/2}$ at 83.96 eV).[35] Error of binding energies of elemental lines are estimated to be ±0.2 eV.

Other Techniques. Experimental details for the pyrite water solubility determination, Raman microscopy, X ray powder diffraction, ζ potential measurements, and speciation calculations are given in the Supporting Information (SI).

RESULTS AND DISCUSSION

Batch Experiments. Figure 1 summarizes the batch experiments of ^{99}Tc(VII) removal by pure synthetic pyrite. Figure 1a shows the pH effect on the Tc immobilization by pyrite for 42 days. Tc removal (97−100%) from the solution is achieved after 1 day at pH > 5.50 ± 0.08 ($\log K_d$ = 5.0 ± 0.1), whereas at pH < 5.50 ± 0.08 the Tc retention kinetics are significantly slower, being complete only after 35 days ($\log K_d$ = 4.5 ± 0.1). For the kinetics and pH effect experiments, the initial Tc concentration was 5×10^{-6} M and the average final concentration was 5×10^{-8} M.

It is noteworthy to mention that Tc removal at pH 4.50 ± 0.05 is lower than at any other evaluated pH value in the experiments for contact times shorter than 35 days. The same effect was observed in a paper about ReO_4^- retention on pyrite,[36] although the yield of Re removal was lower than in our case with Tc. To analyze if pyrite dissolution was responsible for this observation, FeS_2 solubility was studied as a function of pH by inductively coupled plasma mass spectrometry (Figure S2). The highest Fe concentration in solution was found at pH = 4.50 ± 0.05 and it decreases drastically when pH becomes alkaline, which is in agreement with the results of Bonnissel Gissinger et al.,[27] who reported the formation of Fe(III) (hydr)oxides on the pyrite surface as pH increases, hindering pyrite dissolution.

Cui et al.[37] concluded that Tc(VII) reduction by Fe^{2+} in solution is kinetically unfavorable, while the process is faster if the iron is presorbed on a mineral phase or takes part of the structural solid.[24,37−39] Considering these kinetic implications and the fact that most of the measured Eh values lie in the stability region of Tc(IV) (Figure 1b), suggesting that Tc(VII) was reduced to Tc(IV) by pyrite, the higher pyrite dissolution observed at pH 4.50 ± 0.05 is responsible for the slower Tc uptake by pyrite.

Tc removal by pyrite in water and 0.1 M NaCl after 14 days of interaction was compared in the pH range from 3.50 to 10.50 (Figure 1c). It slightly decreased at acidic pH values, which could be related to outer sphere complexation, as it appears to be dependent on the ionic strength. However, for higher pH values, the Tc uptake is not affected by the increase of ionic strength, which rules out outer sphere complex formation. The slight difference in the Tc removal at acidic pH values could rather be explained by the higher solubility of TcO_2 and Tc(IV) aqueous species when ionic strength rises,[40,41] assuming that it is formed in small amounts after the reduction of Tc(VII) and that the soluble Tc(IV) does not sorb on pyrite.

To evaluate if Tc(IV) immobilized by pyrite reoxidizes to Tc(VII), two samples at pH 6.00 ± 0.07 and 10.00 ± 0.04 have been exposed to oxygen. First, it was ensured that the initial load of Tc was removed from the solution, i.e., the technetium concentration decreased from 5 to 0.041 mM at pH 10.00 ± 0.04 and 0.046 mM at pH 6.00 ± 0.07 after 5 days in contact with pyrite. As the system was kept under constant agitation and was opened several times for pH adjusting and sampling, the amount of oxygen required to reoxidize Tc(IV) was rapidly reached. Moreover, as the pyrite surface was already oxidized (shown in the pyrite Experimental section), it was expected that the oxygen added to the suspensions reacted preferably with Tc instead of the mineral. Furthermore, according to the published pyrite oxidation rates,[42] all pyrite should be fully oxidized by the end of the reoxidation experiments (57 days). However, such calculated oxidation rates should be critically considered, since the pyrite oxidation rate may be increased by the presence of Fe(III) and additionally affected by other oxidants in the solution, i.e., Tc(VII).

Figure 1d shows that the technetium concentration in the solution remained lower than 1 μM at both pH values after direct contact with oxygen for 2 months, suggesting that pyrite will prevent further Tc migration through the biosphere. However, Figure S3 of the Supporting Information indicates slightly different behaviors for the two pH values: on the one hand, at pH 10.00 ± 0.04, the maximal amount of Tc in solution, $\%Tc_{sol}$, is found at 7 days, going from 8.0 to 11.0%; after 7 days it decreases again and stays steadily below 5% for the remaining time of the experiment. At pH 6.00 ± 0.07, on the other hand, the maximal release of Tc to the solution occurs at 57 days, where the $\%Tc_{sol}$ reaches 13.5%.

The behavior at pH 10.00 ± 0.04 could indicate the reoxidation of Tc(IV) after 7 days under aerobic conditions. As $\%Tc_{sol}$ significantly decreases after 22 days, it is possible that the Tc(VII) released into the solution is reduced again by pyrite, whose surface is highly dynamic and does not get passivated against further oxidation even when a layer of iron(III)(hydr)oxides is formed on it.[27,43] The increase of

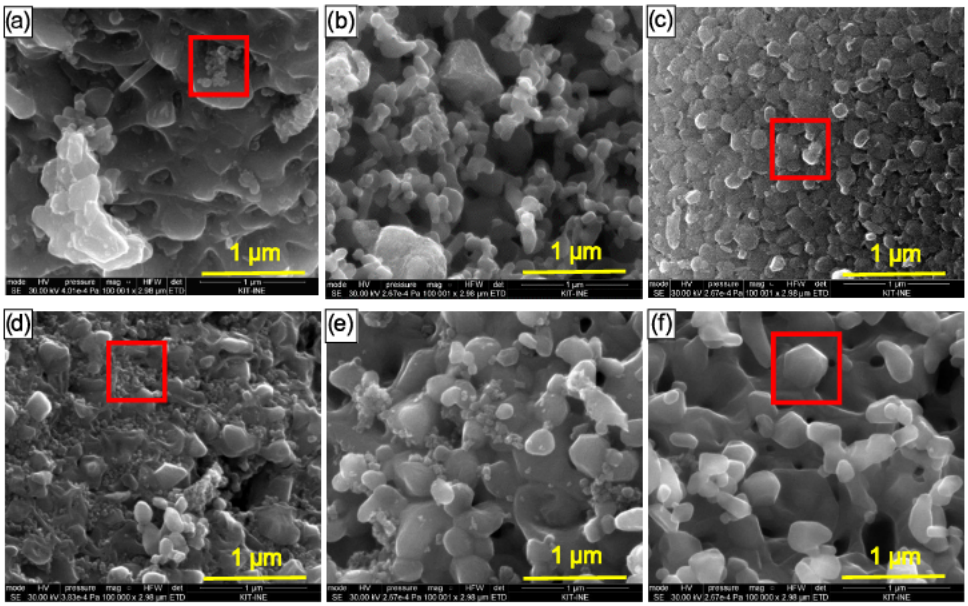

Figure 2. SEM micrographs of pyrite. (a) Pyrite in water at pH 6.00 ± 0.07. (b) Pyrite in water containing 600 ppm Tc load at pH 6.00 ± 0.07. (c) Pyrite in water containing 1000 ppm Tc load at pH 6.00 ± 0.07. (d) Pyrite in water at pH 10.00 ± 0.04. (e) Pyrite in water containing 600 ppm Tc load at pH 10.00 ± 0.04. (f) Pyrite in water containing Tc 1000 ppm Tc load at pH 10.00 ± 0.04. Highlighted in red: (a, d): small particles suggesting new iron mineral formation. (c) Possible hematite. (f) Possible magnetite. Contact time with Tc: 1 month.

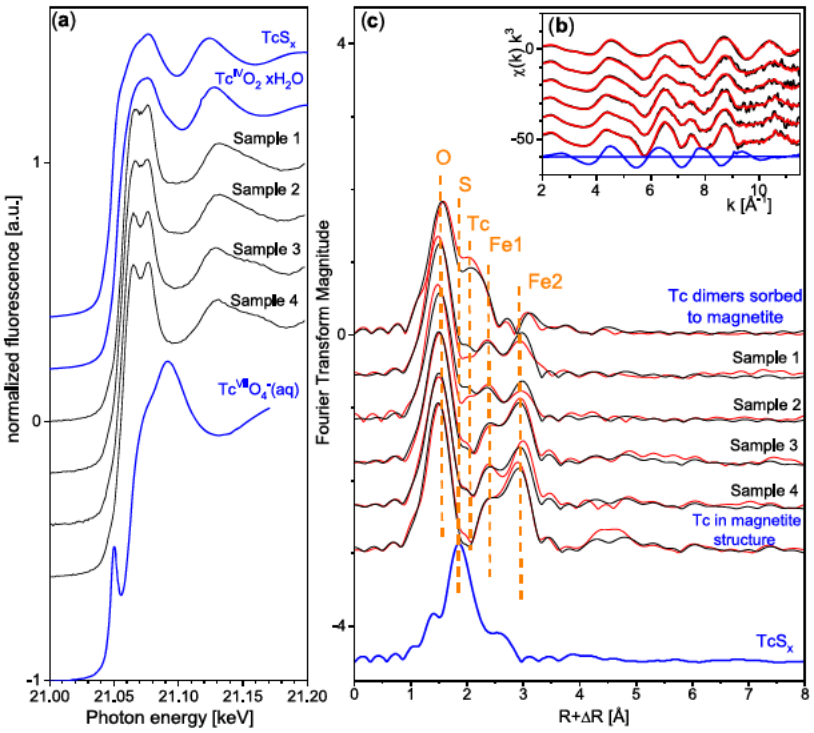

Figure 3. Tc K edge XAS spectra of Tc sorbed on pyrite (a). XANES (b). k_3 weighted EXAFS spectra (c) corresponding to Fourier Transform Magnitude. Black lines represent the experimental data; the red lines in (b) and (c) represent their ITFA reconstruction with two principal components. Spectra of the ITFA derived endmember components are labeled in red. Reference spectra not used for ITFA are shown in blue. The shell fit data of the two endmember components are given in Table 3, and the shell fitting of the identities of the samples 1−4 are given in Table 2.

$\%Tc_{sol}$ at pH 6.00 ± 0.07 is significantly higher than at pH 10.00 ± 0.04 (12.4% at pH 6 ± 0.07 and 6.3% at pH 10.00 ± 0.04 when subtracting the lowest point from the highest in the plots of Figure S3), suggesting that the immobilization of Tc by pyrite at pH 6.00 ± 0.07 is not effective anymore after 57 days in contact with oxygen. However, Figures 1d and S3 show no clear trend of $\%Tc_{sol}$ vs time; moreover, the behavior observed at pH 10.00 ± 0.04 points to a new reduction of Tc(VII) by a still reactive pyrite. Therefore, studies on a considerably longer time scale should be performed to elucidate how long the Tc immobilization capacity of pyrite is at these pH values.

Scanning Electron Microscopy. Figure 2 shows the micrographs of pyrite before and after the reaction with

Table 2. Species Quantification by ITT (Bold Fixed)

sample	no	species 1 (Tc(IV) dimers)	species 2 (structural Tc)	sum
pyrite + Tc 600 ppm pH 6	1	0.86	0.14	1.00
pyrite + Tc 1000 ppm pH 6	2	1.00	0.00	1.00
pyrite + Tc 600 ppm pH 10	3	0.08	0.92	1.00
pyrite + Tc 1000 ppm pH 10	4	0.30	0.70	1.00
magnetite structure	**5**	**0.00**	**1.00**	**1.00**

technetium at pH 6.00 ± 0.07 and 10.00 ± 0.04. Before Tc addition, the pyrite surface at both pH values appears to be quite similar, although at pH 10.00 ± 0.04, more small particles (highlighted in red in micrographs 2a and 2d) are shown. They can be attributed to new iron minerals, like magnetite, hematite, and goethite, formed in the pyrite surface due to its initial oxidation. EDX analysis was not able to find the technetium on the samples, which was attributed to its low concentration.

The interaction with technetium causes a significant change in the morphology of the mineral, especially for the small particles that disappear after the Tc addition while the surface becomes smoother. This change is more pronounced with the increase in the Tc concentration, implying that it is a consequence of the redox reaction.

Micrographs 2c and 2f show the pyrite surface at pH 6.00 ± 0.07 and pH 10.00 ± 0.04 after the interaction with 1000 ppm Tc for 1 month. There is a clear difference between the surfaces at each pH value, suggesting that the iron minerals formed with the Tc reduction are not the same. A visual comparison between our results and the micrographs obtained by Taitel Goldman[44] (Figure S4) shows that the surfaces resemble hematite at pH 6.00 ± 0.07 and magnetite at pH 10.00 ± 0.04.

Raman microscopy was used to identify the minerals formed. However, this was only possible with the sample of pyrite containing 1000 ppm Tc load at pH 6.00 ± 0.07 (Figure S5), where hematite was recognized by comparison with the reference R050300 of the RRUFF database.[26]

X-ray Absorption Spectroscopy. Figure 3 summarizes the Tc K edge XAS spectra of the Tc(VII) reacted pyrite samples. The XANES spectra (Figure 3a) of all samples are identical. The position is in line with Tc(IV) as a comparison with the $TcO_2{\cdot}xH_2O$ reference spectrum shows. The easily detectable pre edge peak of Tc(VII) is absent in all samples, indicating that Tc(VII) amounts to less than 2%. Comparison with the spectrum of the Tc(IV) sulfide, TcS_x, demonstrates that Tc in all samples is prevalently coordinated to oxygen and not to sulfur (Figure 3c).

Figure 3c shows the Fourier transform magnitude (FTM, which can be seen as a pseudoradial distribution function of atoms around Tc centers) of the four samples along with two Tc references shown above and below, representing Tc(IV) dimers sorbed to magnetite ($Fe^{II}Fe_2^{III}O_4$) and Tc(IV) substituting for Fe in the octahedral position of magnetite (structural Tc), respectively.[10] The samples at pH 6.00 ± 0.07 (samples 1 and 2) show some similarity with the sorption complex, while samples at pH 10.00 ± 0.04 (samples 3 and 4) are similar to structural Tc, although there remain significant differences to the two references. Principal component analysis performed with iterative transformation factor analysis (ITFA) software[33] shows that the four sample spectra can be reconstructed with two principal components (red lines), indicating that Tc occurs in only two different local structures.

To test whether any of the available references are in line with the two components present in the sample spectra, we repeated the principal component analysis by adding the available reference spectra[10,45] to the four samples. Addition of $TcO_2{\cdot}xH_2O$, TcS_x, or Tc dimers sorbed on magnetite always resulted in an increase of the number of significant spectral components to three, indicating that they do not constitute one of the two components present in the samples (not shown).

Uptake of Tc(IV) substituted on octahedral sites of magnetite, however, did not increase the number of components and provided a reasonable fit of all five spectra (samples plus Tc in the magnetite structure in Figure 3c). The incorporation of Tc(IV) into magnetite has been previously observed[10,11] and is explained by Tc^{4+} and Fe^{3+} having identical crystal radii (0.785 Å) in six fold coordination,[46] and Fe^{2+} providing a reasonable charge compensation for Tc^{4+}[47,48] and, therefore, Tc removal by pyrite at pH 10.00 ± 0.04 can be assigned to this incorporation process.

Based on the identification of one of the two endmember components, we performed an iterative transformation target test with ITFA to derive the fraction of the two components in the sample spectra (by fixing the fraction of structural Tc to unity) and to derive the endmember spectrum of the second component (Table 2). The visual appearance of the spectra (Figure 3b,c) suggests that samples at pH 10.00 ± 0.04 consist predominately of species 2 (structural Tc), whereas samples at pH 6.00 ± 0.07 are mainly constituted by species 1, which is similar but not identical to a Tc sorption complex.

To identify species 1, we performed the shell fitting of its spectrum, as shown in Table 3 (Figure S6). First, we

Table 3. EXAFS Derived Structural Parameters for Tc in the Pyrite Samples[c]

sample	path	CN[a]	R (Å)	σ^2 (Å^2)	ΔE^0 (eV)	%R[b]
species 1	Tc O	5.8	2.00	0.0046	2.9	8.6
(sorbed Tc(IV) dimers)	Tc Tc	1.3	2.55	0.0100		
	Tc Fe_1	1.9	3.07	0.0098[c]		
	Tc Fe_2	2.7	3.55	0.0098[c]		
species 2	Tc O	6[f]	2.01	0.0043	3.0	6.1
(structural Tc(IV))	Tc Fe_1	6[f]	3.08	0.0113		
Yalçıntaş[10]	Tc Fe_2	6[f]	3.49	0.0093		

[a]CN, coordination number. [b]R, residual. [c]Fit errors: CN: ± 25%; R: 0.01 Å, σ^2: 0.002 Å^2, f: fixed, c: constrained.

conducted the fit with one Tc−O and two Tc−Fe shells following the visual appearance of only two Tc−Fe shells in the FTM. This fit, however, strongly deviated from the experimental spectrum. Therefore, we added an additional Tc−Tc shell, which was found before to be essential for a reliable fit.[10] In agreement with this former fit regime, we obtained a reliable match of the spectrum of component 1.

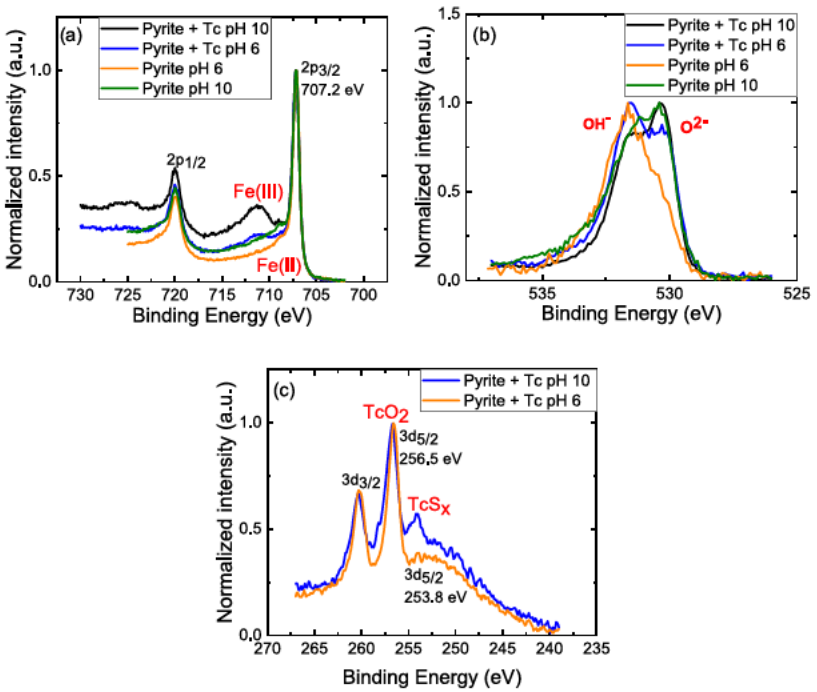

Figure 4. XPS spectra of pyrite after the reaction with Tc(VII) ([Tc] = 1000 ppm) at pH 6.00 ± 0.07 and pH 10.00 ± 0.04. (a) Fe 2p. (b) O 1s. (c) Tc 3d. Tc 3d elemental lines are superposed by the broad loss line of S 2s.

Such obtained structural parameters again suggest the sorption of Tc−Tc dimers on an iron oxide surface. In contrast to the similar sorption complex found after the reaction of Tc with magnetite, the first Tc−Fe distance is 0.05 Å shorter, and the second Tc−Fe distance is 0.03 Å longer,[10] which implies that the dimers are not sorbed on magnetite.

Based on our SEM and Raman microscopic results (Figure S6), we propose that the iron mineral interacting with Tc at pH 6.00 ± 0.07 is hematite, that has already been probed to form surface complexes with Tc(IV) dimers.[49−51] The iron speciation under the experimental conditions ($[TcO_4^-]$ = 5 μM; $[Fe^{2+}]_{Total}$ = 20 μM) was calculated (Figure S7). As a result of the Fe(III) formation when technetium is reduced, the model predicts the formation of hematite at pH < 7.50 and magnetite at pH > 7.50. Even though the simulation assumes that the reduction of Tc is homogenous and completed at pH 4.50, it supports our findings of Tc incorporation into magnetite at pH 10.00 ± 0.04 and the dimer sorption onto hematite at pH 6.00 ± 0.07.

X-ray Photoelectron Spectroscopy. Figure 4 shows the XPS spectra of the sample at pH 6.00 ± 0.07 and 10.00 ± 0.04. There is no visible change in the S 2p spectra (Figure S8), while the formation of Fe(III) is observed at the Fe 2p spectra (Figure 4a), confirming that iron is the redox sensitive element of the pyrite. Fe(III) formation increases with increasing pH and technetium load.

O 1s spectra (Figure 4b) show that the $[O^{2-}]/[OH^-]$ ratio depends on the pH, favoring $[OH^-]$ at pH 6.00 ± 0.07 and $[O^{2-}]$ at pH 10.00 ± 0.04. This is in good agreement with the results reported in previous works[27,52,53] according to which increasing the pH leads to the formation of Fe(III) (hydr)oxides that cover the pyrite surface without passivating it against further oxidation. The new Fe(III) layer shows that O H groups exist on the pyrite surface. These O H groups are probably involved in the inner sphere sorption complexes formed at pH 6.00 ± 0.07 between Tc dimers and the hematite, as found by EXAFS.

Figure 4c shows the Tc 3d spectra at pH 6.00 ± 0.07 and 10.00 ± 0.04. The main difference between both pH values is the peak around 254 eV at pH 10.00 ± 0.04, which indicates the formation of TcS_x. Even though the concentration of this species is too low to be detected by XAS, the XPS spectra show that its concentration increases with the technetium concen tration and may be more relevant in the Tc uptake at higher pH values. The particular surface sensitivity of XPS may have caused the detection of a most likely small fraction of TcS_x, which is not visible by the bulk technique EXAFS. Due to its association with the pyrite surface, this species could be a surface complex and, hence, constitute a transient phase in the total redox process; more studies should be carried out on this matter. The TcS_x found in this work shows that it is very relevant to study the Tc removal by sulfur minerals (like chalcocite, galena, or chalcopyrite), as they are redox sensitive and they might be alternatives for Tc remediation. Indeed, previous works with mackinawite[10] and microorganisms[54] have reported the formation of TcS_x or polysulfide aqueous species that, due to their low solubility,[55] are responsible for Tc remediation.

Environmental Significance. Pyrite, the most common sulfur mineral in the earth's crust, is widely distributed in several geological formations like sedimentary deposits, hydrothermal veins, and metamorphic rocks. We have shown that it removes technetium from water in a wide pH range, being faster at pH ≥ 5.50 ± 0.08, where the Tc uptake yield is 100% within 1 day.

In the environment, Tc is usually found in concentrations around 1 × 10^{-9} M,[56,57] which is around three magnitude orders lower than the concentration used in this study. However, the isotherms shown in Figure S9 of the Supporting Information indicate that the Tc removal by pyrite at both pH 6.00 ± 0.07 and 10.00 ± 0.04 increases when the Tc

concentration decreases, making our results also valid for a more realistic scenario.

The mechanism of removal is highly influenced by the pH, which promotes the formation of hematite and magnetite (among other Fe minerals) on the pyrite surface. Even though the surface is already oxidized, the Fe^{2+} in the bulk of the mineral promotes the Tc(VII) reduction to Tc(IV), which is subsequently followed by the formation of an inner sphere sorption complex between hematite and Tc(IV) dimers at pH 6.00 ± 0.07, while at pH 10.00 ± 0.04, Tc(IV) is incorporated into magnetite, replacing an Fe in an octahedral position.

Lukens et al.[58] studied the leaching of Tc(IV) incorporated into magnetite after oxygen exposure. They found that after 60 days in contact with aerated water, around 10% of technetium had been released from pure magnetite, which is clearly not the case in our study, where the magnetite is formed on the pyrite surface (Figures 1d and S3). This result highlights the role of pyrite in the immobilization: it does not only provide Fe^{2+} for the reduction but also sustains a dynamic surface on which magnetite, among other Fe phases, is continuously formed. The fact that the surface is not passivated ensures that even if Tc(IV) is reoxidized and released to the solution, there will be enough Fe^{2+} to reduce it again and it can be incorporated again by the freshly formed magnetite. At pH 6.00 ± 0.07, however, a significantly higher $\%Tc_{sol}$ was found after 57 days. As the plots in Figures 1d and S3 are not following a clear trend, it is not possible to predict if the $\%Tc_{sol}$ will increase or decrease with time at any of the two pH values.

Nevertheless, due to the fast kinetics of removal in a wide range of pH and its ability to retain technetium under aerobic conditions for a sufficient period, pyrite should be considered for the remediation of contaminated waters, as it could remove technetium (and probably other pollutants) in the same way that activated carbon scavenges organic impurities. Moreover, even in the "do nothing" option, effects from natural attenuation are to be expected in the surrounding of nuclear waste repositories like Yucca Mountain, where pyrite is abundant,[59] or repositories using materials like bentonite as host rocks, where pyrite will be found as accessory mineral.[60]

ASSOCIATED CONTENT

Supporting Information

The Supporting Information is available free of charge at https://pubs.acs.org/doi/10.1021/acs.est.9b05341.

Pyrite solubility determination, X ray powder diffraction, ζ potential measurements, Raman microscopy and modeling; pyrite characterization, pH effect on pyrite solubility, pH adjustment; %Tc released to solution during the reoxidation assays; identification of Fe(III) minerals with SEM micrographs; Raman spectra of the pyrite + Tc 1000 ppm at pH 6; shell fit of the sorption complex; calculated iron speciation; S 2p XPS spectra; isotherms (PDF)

AUTHOR INFORMATION

Corresponding Authors

Natalia Mayordomo − *Institute of Resource Ecology, Helmholtz Zentrum Dresden Rossendorf, 01328 Dresden, Germany;* orcid.org/0000 0003 4433 9500; Phone: +49 351 260 3487; Email: n.mayordomo herranz@hzdr.de

Katharina Müller − *Institute of Resource Ecology, Helmholtz Zentrum Dresden Rossendorf, 01328 Dresden, Germany;* orcid.org/0000 0002 0038 1638; Phone: +49 351 260 2439; Email: k.mueller@hzdr.de

Authors

Diana M. Rodríguez − *Institute of Resource Ecology, Helmholtz Zentrum Dresden Rossendorf, 01328 Dresden, Germany*

Andreas C. Scheinost − *Institute of Resource Ecology, Helmholtz Zentrum Dresden Rossendorf, 01328 Dresden, Germany; The Rossendorf Beamline (ROBL), 38043 Grenoble, France;* orcid.org/0000 0002 6608 5428

Dieter Schild − *Institute for Nuclear Waste Disposal, Karlsruhe Institute of Technology (KIT), 76344 Eggenstein Leopoldshafen, Germany;* orcid.org/0000 0001 6034 8146

Vinzenz Brendler − *Institute of Resource Ecology, Helmholtz Zentrum Dresden Rossendorf, 01328 Dresden, Germany*

Thorsten Stumpf − *Institute of Resource Ecology, Helmholtz Zentrum Dresden Rossendorf, 01328 Dresden, Germany*

Author Contributions

This manuscript was written through contributions of all authors. All authors have given approval to the final version of the manuscript.

Funding

Funding from the German Federal Ministry of Economic Affairs and Energy (BMWi) is acknowledged for the VESPA II joint project (02E11607B).

Notes

The authors declare no competing financial interest.

ACKNOWLEDGMENTS

We are very grateful to Jörg Rothe and Kathy Dardenne from the KARA Synchrotron Radiation Source at KIT for their help during the XAS measurements. We also thank Konrad Molodtsov for his help with the Raman microscope, André Roßberg for his help during the XAS experiments, as well as Stephan Weiß, Carola Eckardt, and Sabrina Beutner for their help in the lab work.

REFERENCES

(1) Meena, A. H.; Arai, Y. Environmental geochemistry of technetium. *Environ. Chem. Lett.* **2017**, *15*, 241−263.

(2) Icenhower, J. P.; Qafoku, N. P.; Zachara, J. M.; Martin, W. J. The biogeochemistry of technetium: A review of the behavior of an artificial element in the natural environment. *Am. J. Sci.* **2010**, *310*, 721−752.

(3) Momoshima, N.; Sayad, M.; Yamada, M.; Takamura, M.; Kawamura, H. Global fallout levels of ^{99}Tc and activity ratio of $^{99}Tc/^{137}Cs$ in the Pacific Ocean. *J. Radioanal. Nucl. Chem.* **2005**, *266*, 455−460.

(4) Guérin, B.; Tremblay, S.; Rodrigue, S.; Rousseau, J. A.; Dumulon Perreault, V.; Lecomte, R.; van Lier, J. E.; Zyuzin, A.; van Lier, E. J. Cyclotron Production of ^{99m}Tc: An Approach to the Medical Isotope Crisis. *J. Nucl. Med.* **2010**, *51*, 13N−16N.

(5) Jurisson, S.; Gawenis, J.; Landa, E. R. Sorption of ^{99m}Tc radiopharmaceutical compounds by soils. *Health Phys.* **2004**, *87*, 423.

(6) Leggett, R.; Giussani, A. A biokinetic model for systemic technetium in adult humans. *J. Radiol. Prot.* **2015**, *35*, 297−315.

(7) EPA (Environmental Protection Agency). Radionuclides in Drinking Water: A Small Entity Compliance Guide, United States of America, 2002.

(8) Rard, J.; Rand, M.; Anderegg, G.; Wanner, H. *Chemical Thermodynamics of Technetium*; Sandino, A.; Östhols, E., Eds.; NEA TDB, 1999.
(9) Lieser, K. H.; Bauscher, C. Technetium in the Hydrosphere and in the Geosphere. I Chemistry of Technetium and Iron in Natural Waters and Influence of the Redox Potential on the Sorption of Technetium. *Radiochim. Acta* **1987**, *42*, 205−213.
(10) Yalçıntaş, E.; Scheinost, A. C.; Gaona, X.; Altmaier, M. Systematic XAS study on the reduction and uptake of Tc by magnetite and mackinawite. *Dalton Trans.* **2016**, *45*, 17874−17885.
(11) Kobayashi, T.; Scheinost, A. C.; Fellhauer, D.; Gaona, X.; Altmaier, M. Redox behavior of Tc(VII)/Tc(IV) under various reducing conditions in 0.1 M NaCl solutions. *Radiochim. Acta* **2013**, *101*, 323−332.
(12) Livens, F. R.; Jones, M. J.; Hynes, A. J.; Charnock, J. M.; Mosselmans, J. F. W.; Hennig, C.; Steele, H.; Collison, D.; Vaughan, D. J.; Pattrick, R. A. D.; et al. X ray absorption spectroscopy studies of reactions of technetium, uranium and neptunium with mackinawite. *J. Environ. Radioact.* **2004**, *74*, 211−219.
(13) Liu, Y.; Terry, J.; Jurisson, S. Pertechnetate immobilization with amorphous iron sulfide. *Radiochim. Acta* **2008**, *96*, 823−833.
(14) Icenhower, J. P.; Martin, W. J.; Qafoku, N. P.; Zachara, J. M. The Geochemistry of Technetium: A Summary of the Behavior of an Artificial Element in the Natural Environment, Washington, 2008.
(15) Marshall, T. A.; Morris, K.; Law, G. T. W.; Mosselmans, J. F. W.; Bots, P.; Parry, S. A.; Shaw, S. Incorporation and retention of ^{99}Tc(IV) in magnetite under high pH conditions. *Environ. Sci. Technol.* **2014**, *48*, 11853−11862.
(16) Lee, M. S.; Um, W.; Wang, G.; Kruger, A. A.; Lukens, W. W.; Rousseau, R.; Glezakou, V. A. Impeding ^{99}Tc(IV) mobility in novel waste forms. *Nat. Commun.* **2016**, *7*, 1−6.
(17) Morris, K.; Livens, F. R.; Charnock, J. M.; Burke, I. T.; McBeth, J. M.; Begg, J. D. C.; Boothman, C.; Lloyd, J. R. An X ray absorption study of the fate of technetium in reduced and reoxidised sediments and mineral phases. *Appl. Geochem.* **2008**, *23*, 603−617.
(18) McBeth, J. M.; Lear, G.; Lloyd, J. R.; Livens, F. R.; Morris, K.; Burke, I. T. Technetium Reduction and Reoxidation in Aquifer Sediments. *Geomicrobiol. J.* **2007**, *24*, 189−197.
(19) Burke, I. T.; Boothman, C.; Lloyd, J. R.; Livens, F. R.; Charnock, J. M.; McBeth, J. M.; Mortimer, R. J. G.; Morris, K. Reoxidation Behavior of Technetium, Iron, and Sulfur in Estuarine Sediments. *Environ. Sci. Technol.* **2006**, *40*, 3529−3535.
(20) Rickard, D. *Sulfidic Sediments and Sedimentary Rocks*; Elsevier B.V: Amsterdam, 2012.
(21) Baeyens, B.; Maes, A.; Cremers, A. In situ physico chemical characterisation of Boom Clay. In *Radioactive Waste Management and the Nuclear Fuel Cycle*; Harwood Academic Publishers: New York, 1985; pp 391−408.
(22) Gaucher, E.; Robelin, C.; Matray, J. M.; Négrel, G.; Gros, Y.; Heitz, J. F.; Vinsot, A.; Rebours, H.; Cassagnabère, A.; Bouchet, A. ANDRA underground research laboratory: interpretation of the mineralogical and geochemical data acquired in the Callovian−Oxfordian formation by investigative drilling. *Phys. Chem. Earth, Parts A/B/C* **2004**, *29*, 55−77.
(23) Bruggeman, C.; Maes, A.; Vancluysen, J. The identification of FeS2 as a sorption sink for Tc(IV). *Phys. Chem. Earth, Parts A/B/C* **2007**, *32*, 573−580.
(24) Huo, L.; Xie, W.; Qian, T.; Guan, X.; Zhao, D. Reductive immobilization of pertechnetate in soil and groundwater using synthetic pyrite nanoparticles. *Chemosphere* **2017**, *174*, 456−465.
(25) Lieser, K. H.; Bauscher, C. H. Technetium in the hydrosphere and in the geosphere II. *Radiochim. Acta* **1988**, *44*, 125−128.
(26) Lafuente, B.; Downs, R. T.; Yan, H.; Stone, N. The Power of Databases: The RRUFF Project. In *Highlights in Mineralogical Crystallography*; De Gruyter: Berlin, 2015; pp 1−30.
(27) Bonnissel Gissinger, P.; Alnot, M.; Ehrhardt, J. J.; Behra, P. Surface Oxidation of Pyrite as a Function of pH. *Environ. Sci. Technol.* **1998**, *32*, 2839−2845.
(28) Hu, G.; Dam Johansen, K.; Wedel, S.; Hansen, J. P. Decomposition and oxidation of pyrite. *Prog. Energy Combust. Sci.* **2006**, *32*, 295−314.
(29) Ressler, T. WinXAS: a Program for X ray Absorption Spectroscopy Data Analysis under MS Windows. *J. Synchrotron Radiat.* **1998**, *5*, 118−122.
(30) Ankudinov, A. L.; Rehr, J. J. Relativistic calculations of spin dependent x ray absorption spectra. *Phys. Rev. B* **1997**, *56*, R1712−R1716.
(31) Wright, J. P.; Attfield, J. P.; Radaelli, P. G. Charge ordered structure of magnetite Fe_3O_4 below the Verwey transition. *Phys. Rev. B* **2002**, *66*, No. 214422.
(32) Rodriguez, E. E.; Poineau, F.; Llobet, A.; Sattelberger, A. P.; Bhattacharjee, J.; Waghmare, U. V.; Hartmann, T.; Cheetham, A. K. Structural Studies of TcO_2 by Neutron Powder Diffraction and First Principles Calculations. *J. Am. Chem. Soc.* **2007**, *129*, 10244−10248.
(33) Roßberg, A.; Reich, T.; Bernhard, G. Complexation of uranium(VI) with protocatechuic acid—application of iterative transformation factor analysis to EXAFS spectroscopy. *Anal. Bioanal. Chem.* **2003**, *376*, 631−638.
(34) Rossberg, A.; Ulrich, K. U.; Weiss, S.; Tsushima, S.; Hiemstra, T.; Scheinost, A. C. Identification of uranyl surface complexes on ferrihydrite: Advanced EXAFS data analysis and CD music modeling. *Environ. Sci. Technol.* **2009**, *43*, 1400−1406.
(35) Seah, M. P.; Gilmore, I. S.; Beamson, G. XPS: binding energy calibration of electron spectrometers 5—re evaluation of the reference energies. *Surf. Interface Anal.* **1998**, *26*, 642−649.
(36) Ding, Q.; Ding, F.; Qian, T.; Zhao, D.; Wang, L. Reductive immobilization of rhenium in soil and groundwater using pyrite nanoparticles. *Water, Air, Soil Pollut.* **2015**, *226*, 517.
(37) Cui, D.; Eriksen, T. E. Reduction of pertechnetate by ferrous iron in solution: Influence of sorbed and precipitated Fe(II). *Environ. Sci. Technol.* **1996**, *30*, 2259−2262.
(38) Cui, D.; Eriksen, T. E. Reduction of pertechnetate in solution by heterogeneous electron transfer from Fe(II) containing geological material. *Environ. Sci. Technol.* **1996**, *30*, 2263−2269.
(39) Zachara, J. M.; Heald, S. M.; Jeon, B. H.; Kukkadapu, R. K.; Liu, C.; McKinley, J. P.; Dohnalkova, A. C.; Moore, D. A. Reduction of pertechnetate [Tc(VII)] by aqueous Fe(II) and the nature of solid phase redox products. *Geochim. Cosmochim. Acta* **2007**, *71*, 2137−2157.
(40) Yalçıntaş, E.; Gaona, X.; Altmaier, M.; Dardenne, K.; Polly, R.; Geckeis, H. Thermodynamic description of Tc(IV) solubility and hydrolysis in dilute to concentrated NaCl, $MgCl_2$ and $CaCl_2$ solutions. *Dalton Trans.* **2016**, *45*, 8916−8936.
(41) Hess, N. J.; Xia, Y. X.; Rai, D.; Conradson, S. D. Thermodynamic Model for the Solubility of $TcO_2 \bullet xH_2O$(am) in the Aqueous Tc(IV) Na^+ Cl^- H^+ OH^- H_2O System. *J. Solution Chem.* **2004**, *33*, 199−226.
(42) Williamson, M. A.; Rimstidt, J. D. The kinetics and electrochemical rate determining step of aqueous pyrite oxidation. *Geochim. Cosmochim. Acta* **1994**, *58*, 5443−5454.
(43) Karthe, S.; Szargan, R.; Suoninen, E. Oxidation of pyrite surfaces: a photoelectron spectroscopic study. *Appl. Surf. Sci.* **1993**, *72*, 157−170.
(44) Taitel Goldman, N. Recrystallization Processes Involving Iron Oxides in Natural Environments and In Vitro. In: *Recent Developments in the Study of Recrystalization*; IntechOpen: Rijeka, 2013; p 6.
(45) Saeki, M.; Sasaki, Y.; Nakai, A.; Ohashi, A.; Banerjee, D.; Scheinost, A. C.; Foerstendorf, H. Structural Study on 2,2′ (Methylimino)bis(N,N Dioctylacetamide) Complex with Re(VII) O_4^- and Tc(VII)O_4^- by ^{1}H NMR, EXAFS, and IR Spectroscopy. *Inorg. Chem.* **2012**, *51*, 5814−5821.
(46) Shannon, R. D. Revised effective ionic radii and systematic studies of interatomic distances in halides and chalcogenides. *Acta Crystallogr., Sect. A: Cryst. Phys., Diffr., Theor. Gen. Crystallogr.* **1976**, *32*, 751−767.

(47) Lukens, W. W.; Magnani, N.; Tyliszczak, T.; Pearce, C. I.; Shuh, D. K. Incorporation of Technetium into Spinel Ferrites. *Environ. Sci. Technol.* **2016**, *50*, 13160−13168.
(48) Smith, F. N.; Um, W.; Taylor, C. D.; Kim, D. S.; Schweiger, M. J.; Kruger, A. A. Computational Investigation of Technetium(IV) Incorporation into Inverse Spinels: Magnetite (Fe_3O_4) and Trevorite ($NiFe_2O_4$). *Environ. Sci. Technol.* **2016**, *50*, 5216−5224.
(49) Peretyazhko, T.; Zachara, J. M.; Heald, S. M.; Jeon, B. H.; Kukkadapu, R. K.; Liu, C.; Moore, D.; Resch, C. T. Heterogeneous reduction of Tc(VII) by Fe(II) at the solid water interface. *Geochim. Cosmochim. Acta* **2008**, *72*, 1521−1539.
(50) Jaisi, D. P.; Dong, H.; Plymale, A. E.; Fredrickson, J. K.; Zachara, J. M.; Heald, S.; Liu, C. Reduction and long term immobilization of technetium by Fe(II) associated with clay mineral nontronite. *Chem. Geol.* **2009**, *264*, 127−138.
(51) Peretyazhko, T.; Zachara, J. M.; Heald, S. M.; Kukkadapu, R. K.; Liu, C.; Plymale, A. E.; Resch, C. T. Reduction of Tc(VII) by Fe(II) Sorbed on Al (hydr)oxides. *Environ. Sci. Technol.* **2008**, *42*, 5499−5506.
(52) Weerasooriya, R.; Tobschall, H. J. Pyrite−water interactions: Effects of pH and pFe on surface charge. *Colloids Surf., A* **2005**, *264*, 68−74.
(53) Todd, E. C.; Sherman, D. M.; Purton, J. A. Surface oxidation of pyrite under ambient atmospheric and aqueous (pH = 2 to 10) conditions: electronic structure and mineralogy from X ray absorption spectroscopy. *Geochim. Cosmochim. Acta* **2003**, *67*, 881−893.
(54) Lee, J. H.; Zachara, J. M.; Fredrickson, J. K.; Heald, S. M.; McKinley, J. P.; Plymale, A. E.; Resch, C. T.; Moore, D. A. Fe(II) and sulfide facilitated reduction of $^{99}Tc(VII)O_4^-$ in microbially reduced hyporheic zone sediments. *Geochim. Cosmochim. Acta* **2014**, *136*, 247−264.
(55) Pearce, C. I.; Icenhower, J. P.; Asmussen, R. M.; Tratnyek, P. G.; Rosso, K. M.; Lukens, W. W.; Qafoku, N. P. Technetium Stabilization in Low Solubility Sulfide Phases: A Review. *ACS Earth Space Chem.* **2018**, *2*, 532−547.
(56) Schulte, E. H.; Scoppa, P. Sources and behavior of technetium in the environment. *Sci. Total Environ.* **1987**, *64*, 163−179.
(57) Shi, K.; Hou, X.; Roos, P.; Wu, W. Determination of technetium 99 in environmental samples: A review. *Anal. Chim. Acta* **2012**, *709*, 1−20.
(58) Lukens, W. W.; Saslow, S. A. Facile incorporation of technetium into magnetite, magnesioferrite, and hematite by formation of ferrous nitrate in situ: precursors to iron oxide nuclear waste forms. *Dalton Trans.* **2018**, *47*, 10229−10239.
(59) Weiss, S. I.; Larson, L. T.; Noble, D. C. Pyritic Ash Flow Tuff, Yucca Mountain, Nevada − A Discussion, United States of America, 1994.
(60) Diener, A.; Neumann, T.; Kramar, U.; Schild, D. Structure of selenium incorporated in pyrite and mackinawite as determined by XAFS analyses. *J. Contam. Hydrol.* **2012**, *133*, 30−39.

New insights into ^{99}Tc(VII) removal by pyrite: A spectroscopic approach

Diana M. Rodriguez[1], Natalia Mayordomo[1], Andreas C. Scheinost[1,2], Dieter Schild[3], Vinzenz Brendler[1], Katharina Müller[1*], Thorsten Stumpf[1]*

[1] Institute of Resource Ecology, Helmholtz-Zentrum Dresden - Rossendorf, Bautzner Landstraße 400, 01328 Dresden, Germany

[2] The Rossendorf Beamline (ROBL), 71, Avenue des Martyrs, 38043 Grenoble, France

[3] Institute for Nuclear Waste Disposal, Karlsruhe Institute of Technology (KIT), Hermann-von-Helmholtz-Platz 1, 76344 Eggenstein-Leopoldshafen, Germany

Catalogue of Supporting Information:

Detailed information about pyrite solubility determination, X-ray powder diffraction, ζ-potential measurements, Raman microscopy and modelling

Pyrite solubility.

Eight suspensions of pyrite in water (1.3 g L^{-1}) were prepared and their pH was adjusted in the range from 3.50 to 10.50. The samples were equilibrated under horizontal shaking for 3 weeks until the pH was constant. Afterwards, they were centrifuged (600 × g for 1 hour) and an aliquot of 1 mL from the supernatants was acidified with 10 µL of concentrated HNO_3. The Fe^{2+} concentration in each sample was measured by inductively coupled plasma mass spectroscopy, ICP-MS (NexION 350x, Perkin Elmer).

X-ray powder diffraction (XRD)

The synthetic pyrite powder was analyzed by XRD (MiniFlex 600 powder XRD, by Rigaku) using Cu Kα (λ = 1.54184 Å) as X-ray source, that has an X-ray generation of 40 kV / 15 mA (600 W). The spectrum was recorded in a scan continuous mode. The sample preparation was carried out inside a N_2 glove box, where the solid was homogenized with an agate mortar and then mounted on an air-tight sample holder (Rigaku) to ensure the inert conditions of the sample during the measurement.

ζ-potential measurements

In a N_2 glove box, 0.05 g L^{-1} pyrite suspensions were prepared in 0.1 M NaCl between pH 3.00 and pH 10.50. Subsequently, aliquots of the suspension were transferred into disposable cuvettes (DTS1070, Malvern). The cuvettes were taking out of the glovebox, where the ζ-potential measurements were rapidly performed (Zetasizer Nano Series Nano-ZS, Malvern Instruments) at 25 °C. Five different scans

of 30 seconds were carried out for every sample. The presented values are calculated as an average of the five independent measurements.

Raman microscopy. The samples used for these experiments come from the preparation described in the XPS section. Approximately 10 µL of the re-suspension were deposited on a CaF_2 Raman window under inert atmosphere. Once the solid was dry, the cell was sealed to ensure inert atmosphere during the measure. Raman microscopy (Horiba, model Aramis) was performed using a He – Ne Laser with a 10-fold objective with a D 0.3 filter, a pin-hole of 500 µm and a slit of 600 µm.

Modeling. Fe speciation calculations were performed by using the code CHESS v 2.4[1] and the two latest reported thermodynamic databases of Fe and Tc.[2,3]

pH adjustment. Preliminary essays showed that with no further treatment, the pH of the pyrite suspension was not stable in the range from 5.50 to 8.50, as it always became acidic due to the pyrite oxidation.[4]

In order to solve this problem, we decided to adjust the pH of all samples two times a week for the duration of the experiments, because in this range of time the variation of pH was already ± 0.15 pH units. To do so, small amounts of 2 M NaOH and/or HCl were added to the systems when required. The added volume did not exceed 10 µL, which ensured that the variation on Tc concentration and ionic strength was small enough to be neglected, having in mind that the volume of the samples was 32 mL and that the pyrite removed almost 100% of the Tc after one day, meaning that only the first pH adjustment was performed before the completion of the reaction.

Table S1 is an example of the pH adjustment for the kinetics experiments. As can be seen, the standard deviation (SD) of the pH of the samples in the problematic range from 5.50 to 8.50 after the pH

adjustment is comparable with the SD of the pH of the samples whose pH did not change in a significant way.

Table S1. pH values of the kinetics experiments.

Day 1	Day 3	Day 7	Day 14	Day 21	Day 24	Day 35	Day 42	pH average	Standard Deviation
3.56	3.57	3.58	3.67	3.63	3.64	3.58	3.61	3.60	0.04
4.56	4.61	4.58	4.68	4.68	4.63	4.53	4.59	4.61	0.05
5.4	5.55	5.54	5.69	5.52	5.66	5.5	5.59	5.56	0.08
6.67	6.42	6.57	6.62	6.59	6.6	6.62	6.54	6.58	0.07
7.43	7.44	7.55	7.55	7.62	7.55	7.48	7.56	7.52	0.06
8.45	8.58	8.4	8.57	8.59	8.57	8.63	8.54	8.54	0.07
9.51	9.49	9.49	9.58	9.49	9.50	9.50	9.58	9.52	0.04
10.61	10.62	10.62	10.62	10.52	10.52	10.57	10.6	10.58	0.04

Pyrite characterization.

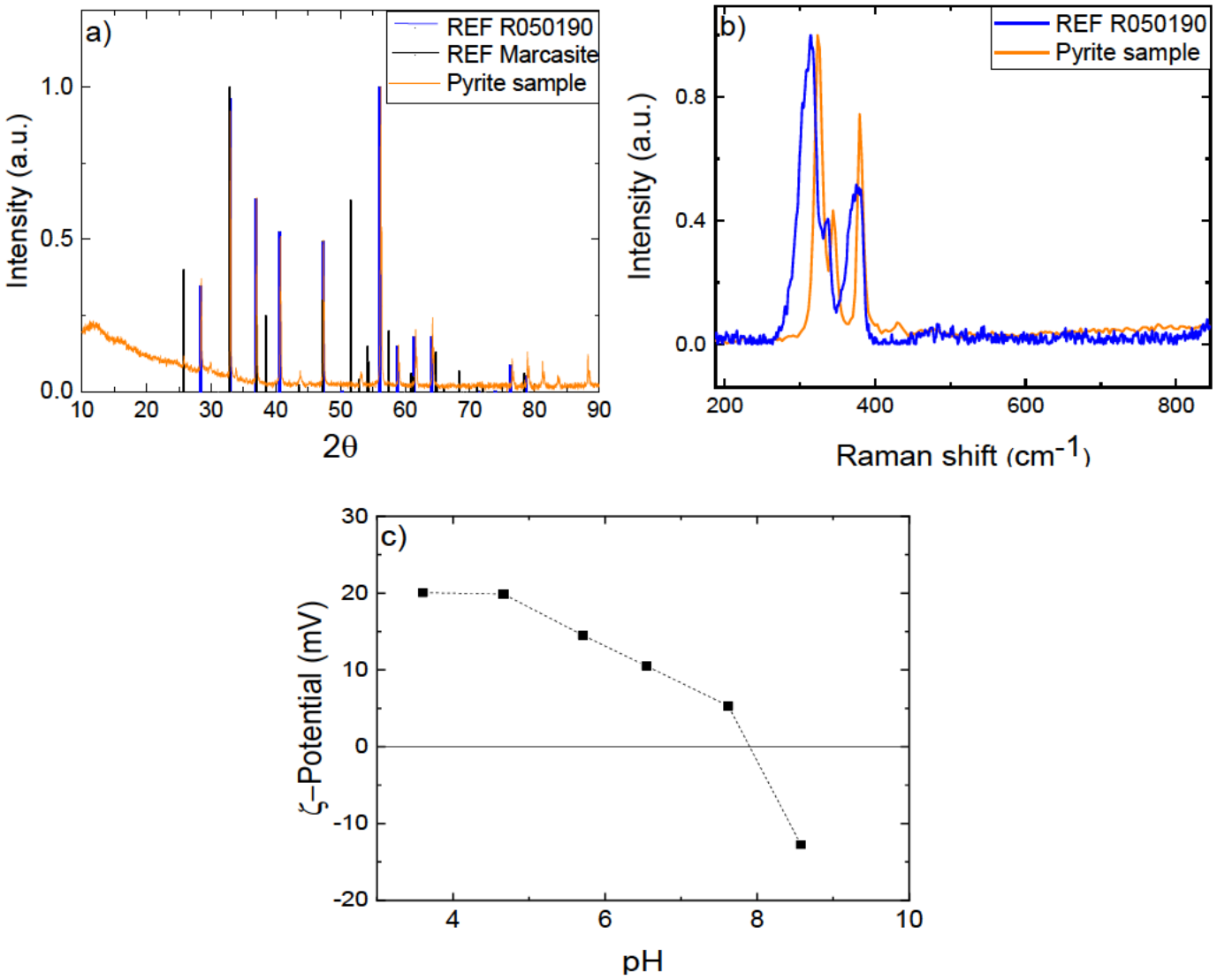

S1. Pyrite characterization experiments. a) Powder XRD, b) Raman microscopy and c) ζ-potential measurements. The references are taken from the RRUFF™ database.[5]

pH effect on pyrite solubility

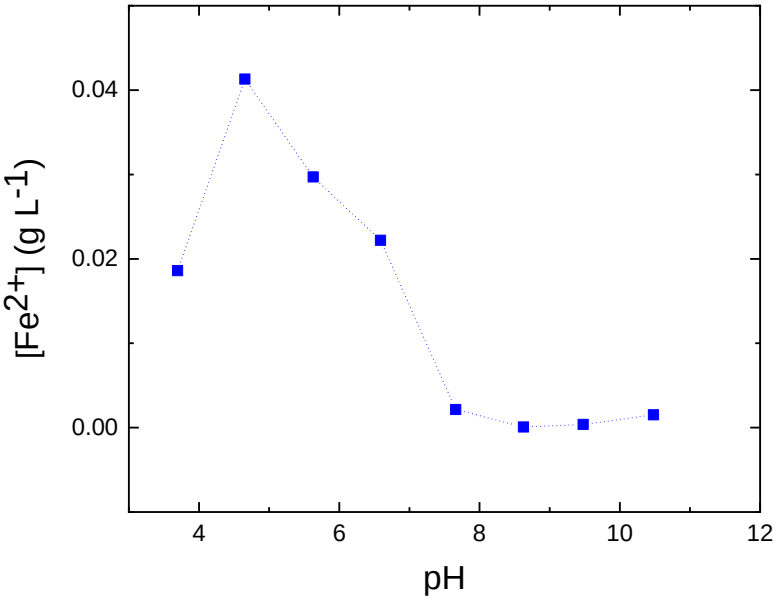

S2. Pyrite solubility measured as Fe concentration as a function of pH studied by ICP-MS (NexION 350x, Perkin Elmer).

%Tc released to solution during the re-oxidation essays

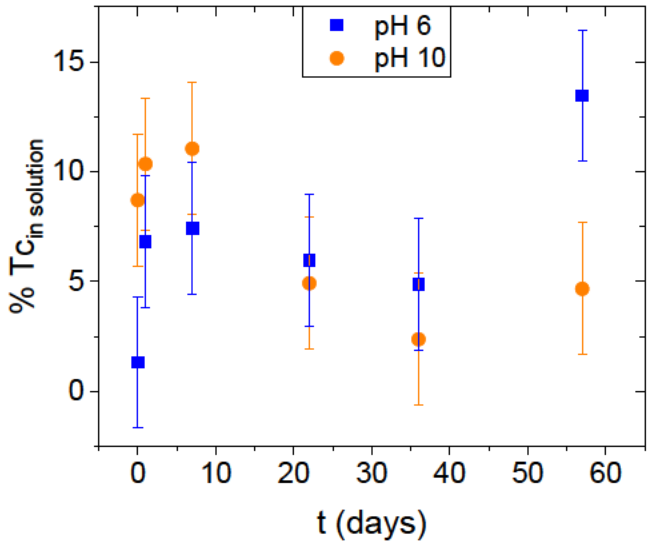

S3. %Tc in solution in the re-oxidation essays performed for 2 months at pH 6.00 and 10.00. %Tc $_{\text{in solution}}$ has been calculated on the basis that the initial Tc concentration (5μM) is 100% of the Tc that might be re-mobilized if re-oxidation occurred in contact with O_2, so the Tc in solution at each time (determined with LSC) is a percentage of this initial Tc concentration.

Identification of Fe(III) minerals with SEM micrographs.

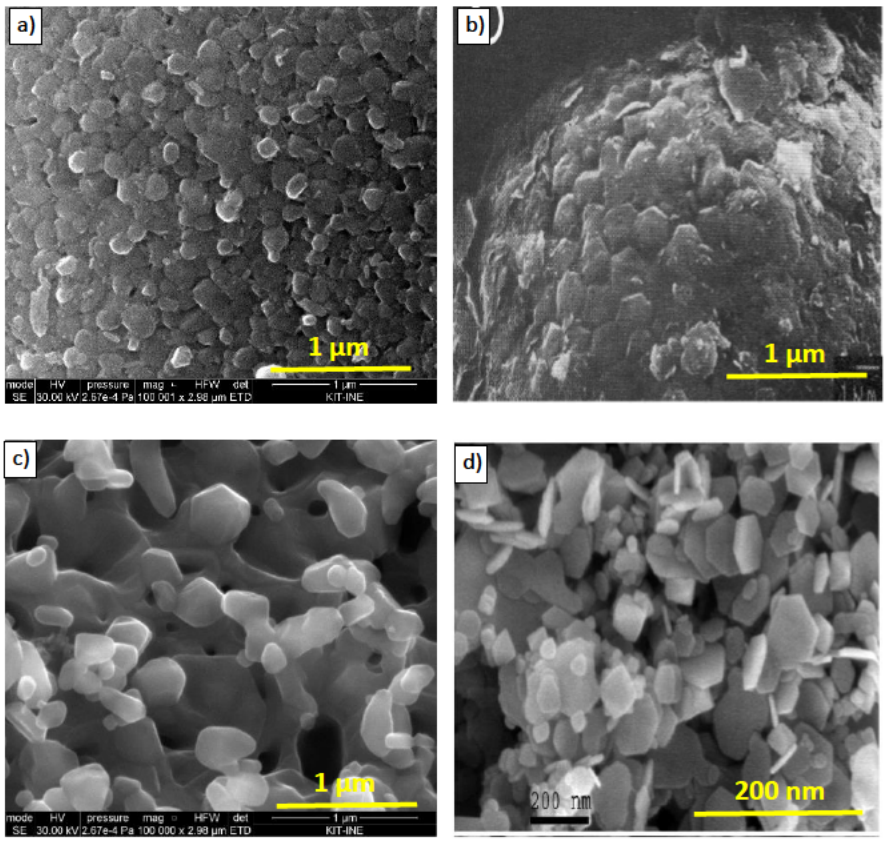

S4. Comparison between the micrographs obtained in this work and the micrographs reported by Taitel-Goldman[6]: (a) this work pH 6.00 ± 0.07 (b) hematite formed by recrystallization of large cubic pyrite crystals[6] (c) this work pH 10.00 ± 0.04 (d) synthesized magnetite at 70°C pH 9.4 and a solution of 4M NaCl[6].

Raman spectra of the pyrite + Tc 1000 ppm at pH 6

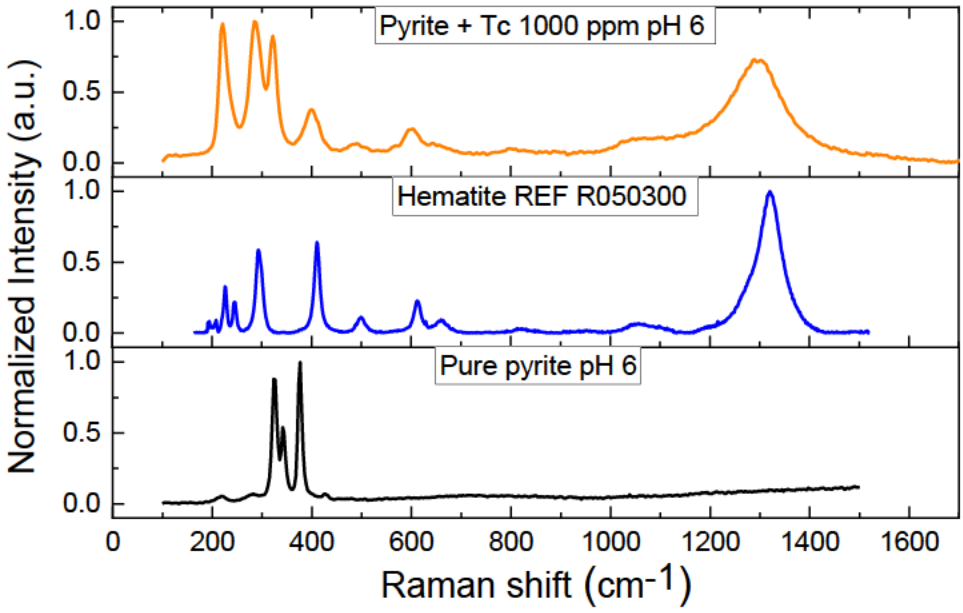

S5. Raman spectra of the pyrite containing 1000 ppm Tc load at pH 6.00 ± 0.07 compared with the hematite reference R050300 of the RRUFF™ database[5] and the spectra of a sample of pyrite at 6.00 ± 0.07 obtained by this work.

Shell fit of the sorption complex

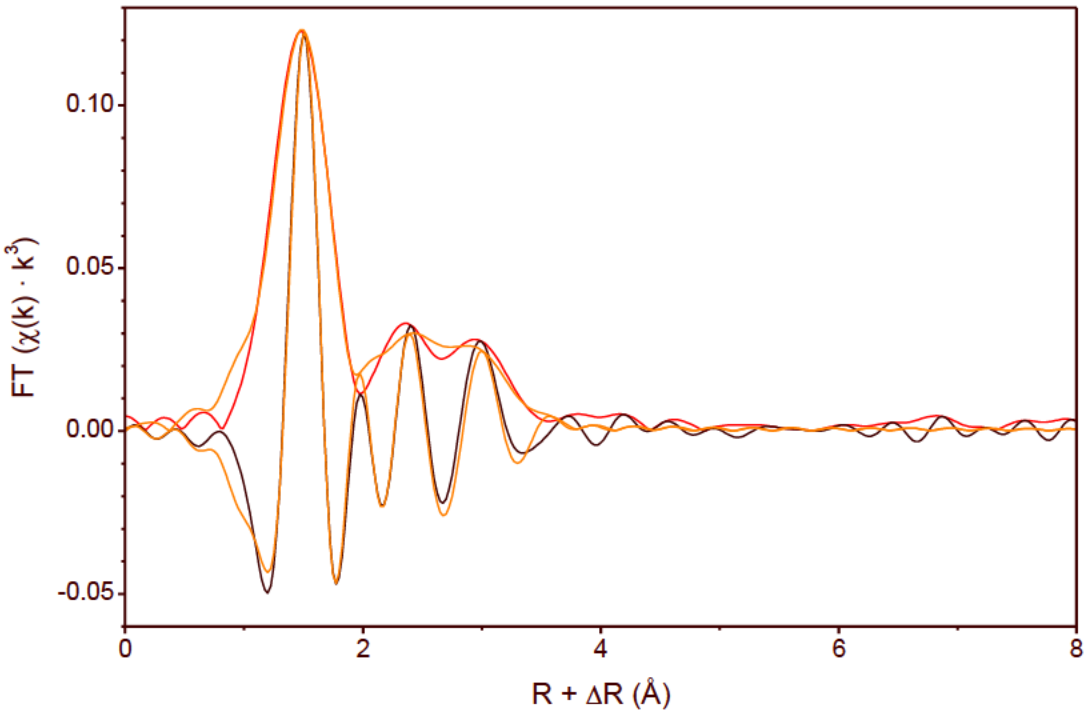

S6. Shell fit of species 1, the sorption complex.

Calculated iron speciation

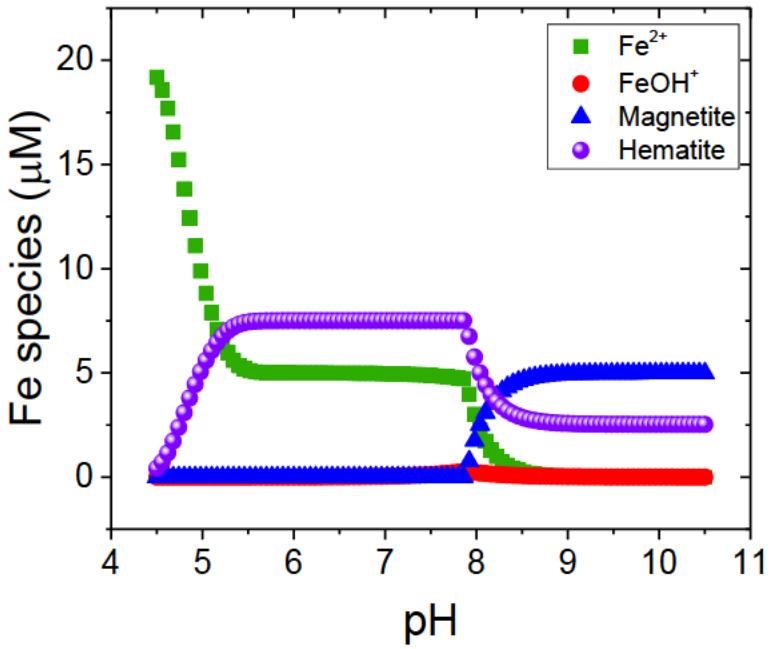

S7. Iron speciation as a function of pH. Calculations have been performed considering the initial presence of 20 μM Fe^{2+} and 5 μM TcO_4^-.The latest Fe [2] and Tc [3] thermodynamic databases have been used.

S 2p XP spectra

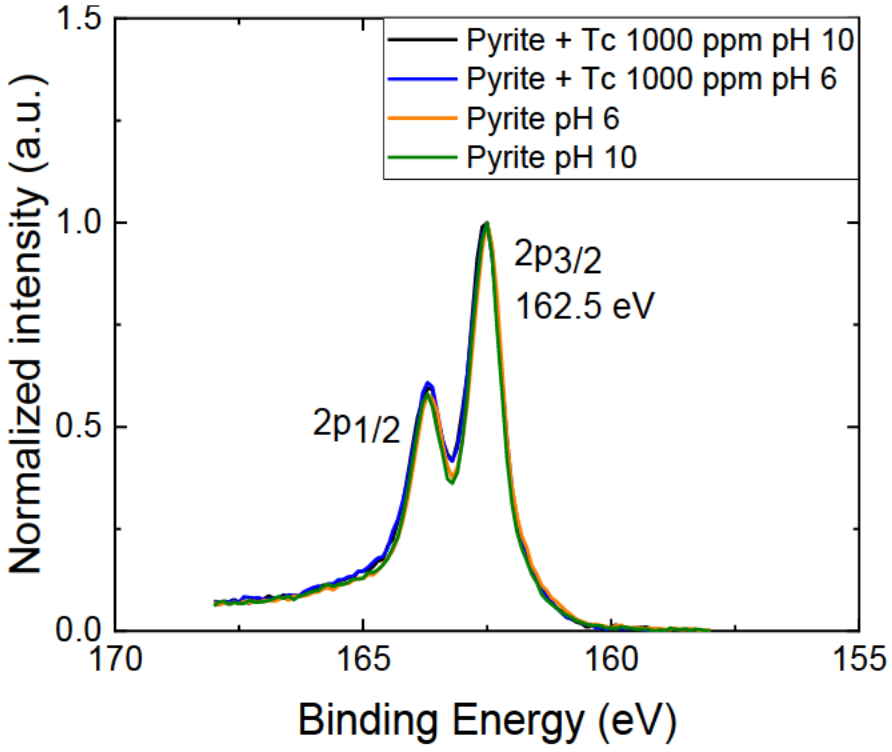

S8. S 2p XP spectra of pyrite after the reaction with Tc(VII) at pH 6.00 ± 0.07 and 10.00 ± 0.04.

Isotherms

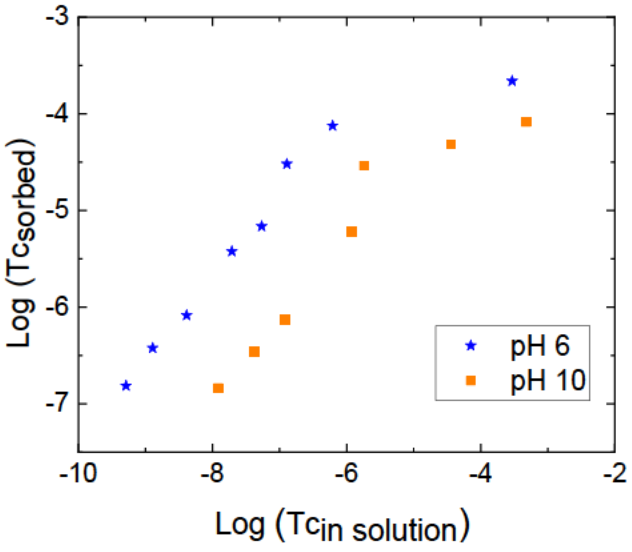

S9. Isotherms of the Tc immobilization by pyrite at pH 6.00 ± 0.07 and 10.00 ± 0.04. The $Tc_{in\ solution}$ is given by converting the activity of the sample (measured by LSC) from Bq mL^{-1} to mol L^{-1}. The Tc_{sorbed} (given in mol g^{-1}) is calculated by subtracting the $Tc_{in\ solution}$ from the initial Tc concentration ($5 \cdot 10^{-6}$ mol L^{-1}) and dividing the result by the pyrite suspension concentration (1.3 g L^{-1}).

References

(1) van der Lee, J.; de Wint, L. Chess Tutorial and Cookbook, Technical Report LHM/RD/99/05. 1999.

(2) Lemire, R. J.; Berner, U.; Musikas, C.; Palmer, D. A.; Taylor, P.; Tochiyama, O. *Chemical Thermodynamics of Iron. Part 1*, OECD Nuclear Energy Agency.; OECD: Paris, France, 2013; Vol. 13a.

(3) Guillaumont, R.; Fanghänel, T.; Neck, V.; Fuger, J.; Palmer, D. A.; Grenthe, I.; Rand, M. H. *Update on the Chemical Thermodynamics of Uranium, Neptunium, Plutonium, Americium and Technetium*; Mompean, F. J., Illemassene, M., Domenech-Orti, C., Ben Said, K., Eds.; OECD: Issy-les-Moulineaux (France), 4, 2003.

(4) Bonnissel-Gissinger, P.; Alnot, M.; Ehrhardt, J.-J.; Behra, P. Surface Oxidation of Pyrite as a Function of pH. *Environ. Sci. Technol.* **1998**, *32* (19), 2839–2845. https://doi.org/10.1021/es980213c.

(5) Lafuente, B.; Downs, R. T.; Yan, H.; Stone, N. The Power of Databases: The RRUFF Project. In *Highlights in Mineralogical Crystallography*; De Gruyter: Berlin, 2015; pp 1–30.

(6) Taitel-Goldman, N. Recrystallization Processes Involving Iron Oxides in Natural Environments and In Vitro; IntechOpen: Rijeka, 2013; p Ch. 6. https://doi.org/10.5772/53735.